# Implementation of an inpainting filter to mitigate the effect of glitches on gravitational-wave parameter estimation

Viviana A. Cáceres Barbosa
*Physics Department, University of Puerto Rico at Mayagüez*

Mentor: Derek Davis
*LIGO, California Institute of Technology*
(Dated: July 28, 2022)

Second Interim Report
LIGO Caltech SURF Program 2022

Recovering accurate distributions for the source parameters of gravitational-wave signals is essential to confirm current models of general relativity and understand astrophysical properties of the universe. Glitches in gravitational-wave strain data may cause a bias in parameter estimation analyses that use Bayesian inference. We implement inpainting to address this problem in `Bilby`, one of various parameter estimation pipelines used for gravitational-wave analyses. Using two different methods to obtain inpainted data, we study how each process affects likelihood evaluation times and `Bilby`'s ability to recover accurate posterior distributions. We will also work towards running different PE analyses using inpainted data with injected signals and studying how often `Bilby` can recover injected parameter values within a specific confidence interval.

## I. INTRODUCTION

Raw strain data recorded by gravitational-wave (GW) detectors such as the Laser Interferometer Gravitational-Wave Observatory (LIGO) is typically dominated by noise coming from a variety of different sources. Although many of these sources are known and well-modeled, there are often short noise bursts, known as glitches, of unknown origin that impact the sensitivity of the data analysis softwares used by the LIGO Scientific Collaboration (LSC) [1]. Much of LSC efforts are dedicated to mitigating the effect of glitches in GW signal searches and parameter estimation (PE) methods.

`Bilby` is one of various PE pipelines used by the LSC [2]. Like most PE pipelines, it uses Bayesian inference to produce posteriors, which are probability distributions of the GW source parameters. These are computed using Bayes' theorem:

$$p(\theta|d) = \frac{\mathcal{L}(d|\theta)\pi(\theta)}{z(d)} \tag{1}$$

where $\mathcal{L}(d|\theta)$ is the likelihood of measuring the data $d$ given some source parameters $\theta$, $\pi(\theta)$ is the prior distribution of these source parameters, and $z(d)$ is the evidence [3].

The `Bilby` analysis assumes that the noise in the data is stationary and Gaussian. This allows the use of the Gaussian noise likelihood [4]:

$$\mathcal{L}(d|\theta) = \frac{1}{|2\pi C|^{\frac{1}{2}}} \exp\left\{-\frac{1}{2}\chi^2(d,h)\right\} \tag{2}$$

with

$$\chi^2(d,h) = [d-h(\theta)]\, C^{-1}\, [d-h(\theta)] \tag{3}$$

where $d$ is a vector representation of the data, $C$ is the noise covariance matrix and $h(\theta)$ is the waveform that depends on parameters $\theta$. In practice, Eq. 2 is costly to compute, so the Whittle approximation to the likelihood is used [5]:

$$\mathcal{L}(d|\theta) \propto \exp\left[-\frac{1}{2}(d-h|d-h)\right] \tag{4}$$

where $(d-h|d-h)$ is the noise-weighted inner product defined as

$$(a|b) \equiv \sum_{j=0}^{\frac{N}{2}-1} 4\,\mathrm{Re}\left(\frac{\tilde{a}_j^* b_j}{S_n(f_j)}\Delta f\right) \tag{5}$$

for a segment with $N$ samples and power spectral density $S_n$.

In this paper we explore cases where these assumptions may not be valid due to the presence of glitches in data. Glitches may create a bias in the likelihood calculations, especially when they occur close to a gravitational-wave signal [6]. Therefore, segments of strongly non-stationary, non-Gaussian data must be dealt with before expressions like Eq. 2 and Eq. 4 can be used.

### A. Inpainting

A method to address the effect of glitches on data analysis using an inpainting filter was derived in [7]

and discussed in the context of PE in [5]. Here we review this derivation and its application to likelihood calculations.

We denote $N_d$ the total number of data samples and $N_h$ the number of data samples in the specified region to be inpainted, known as the *hole*. The inpainting filter $F$ is designed to satisfy

$$u^{(\alpha)T} C^{-1} F d = 0 \tag{6}$$

where $u^{(\alpha)}$ is a list of $N_h$ vectors that are 1 at one of the samples in the hole and 0 elsewhere.

While the matrix for the inpainting filter $F$ can be directly obtained as defined in Eq. 43 of [7], the inpainted data $Fd$ can also be obtained without directly finding $F$ by solving Eq. 6. To do this, the inpainted data can be rewritten as:

$$Fd = d - d_{proj} \tag{7}$$

where $d_{proj}$ is the projection of the hole-region data into the overwhitened data space and 0 elsewhere. If we define the matrix $A$ such that $A_{i,\alpha} = u_i^{(\alpha)}$, then the Toeplitz system,

$$A^T C^{-1} A A^T d_{proj} = A^T C^{-1} d \tag{8}$$

can be solved for $d_{proj}$ in the hole region.

Once the inpainted data is obtained, it can be used for Bayesian analysis. Using the inpainted data and waveform in the Whittle approximation (Eq. 4),

$$\mathcal{L}(d_{inp}|\theta) \propto \exp\left[-\frac{1}{2}(d_{inp} - h_{inp}|d_{inp} - h_{inp})\right] \tag{9}$$

$$= \exp\left[-\frac{1}{2}(d_{inp}|d_{inp}) + (d_{inp}|h_{inp}) - \frac{1}{2}(h_{inp}|h_{inp})\right] \tag{10}$$

Overwhitening corresponds to dividing by the power spectral density $S_n$. By design of the inpainting filter (Eq. 6), when we calculate each of the terms above using Eq. 5, data inside the hole will not contribute to the overall likelihood.

Unlike gating, which is another popular method for glitch mitigation, inpainting does not introduce artifacts outside the hole once the data is whitened. It therefore allows for minimal data corruption. Fig. 1 visually compares gating and inpainting for mitigating the glitch near GW170817. As shown, inpainting effectively reduces the appearance of the glitch and does not modify data outside the specified window.

Here we implement inpainting in `Bilby` and study how this process affects PE analyses. Sec. II A and Sec. II B describe two methods that we use to obtain inpainted data and the computational efficiency of each.

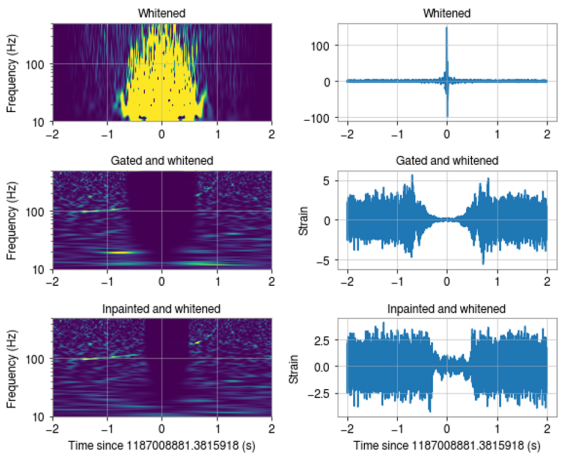


FIG. 1. Glitch near GW170817. Top panel shows the whitened data. Middle panel shows the whitened gated data. Bottom panel shows inpainted data.

Sec. II C shows how we inpaint multiple segments of data. Sec. II D presents the results of different PE runs that have been completed with our methods. Finally, Sec. III and Sec. IV describe the problems we have encountered and our future plans for this project.

With LIGO's increasing sensitivity, having a glitch mitigation method like inpainting implemented in BILBY for future observing runs will be of great value for astrophysical analyses of gravitational waves.

## II. METHODS

As described in Sec. I A, the inpainted data can be obtained either by explicitly finding the $F$ matrix or by solving the Toeplitz system in Eq. 8. Both of these methods were implemented to compare their efficiencies in the context of PE.

### A. Solving for F

To use the $F$ matrix, we calculate each term in Eq. 43 from [7], then apply the filter by multiplying $Fd$. Fig. 2 shows a segment of overwhitened inpainted data that was obtained by directly finding and applying the $F$ matrix to the data. Note that this is an arbitrarily selected segment that did not necessarily contain a glitch. The data within the holes is approximately zero, as we require. The small visible artifacts are most likely due to numerical noise.

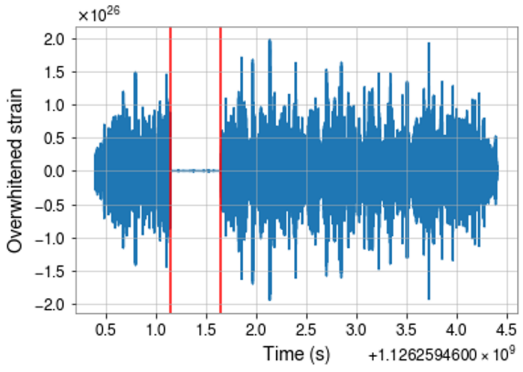


FIG. 2. Overwhitened inpainted data obtained by directly applying F matrix. Red vertical lines specify the region that was modified.

### 1. *Computational efficiency*

To find $F$, the costliest individual step involves inverting a matrix of size $N_h \times N_h$, which has a computational complexity of $\mathcal{O}(N_h^3)$. However, in our analysis, this is done as a pre-processing step for each interferometer's data, so this does not contribute significantly to the run time of a complete analysis. The next costliest operation is the matrix multiplication that applies $F$ to the data and the signal, which is of $\mathcal{O}(N_d^2)$. This is repeated for every sample in the PE analysis and does increase the run time significantly.

We inject a binary black hole (BBH) signal into 4 seconds of data sampled at 4096 Hz and compare the single-likelihood evaluation times with and without inpainting. 30 samples were evaluated for 15 window lengths between 0 and 2 seconds. Fig. 3 shows the ratio between the median evaluation time for each window and the median evaluation time without inpainting.

The evaluation time is approximately constant with increasing windows lengths. This is to be expected since the matrix multiplication depends on $N_d$ rather than $N_h$. The evaluation time increases by 2 orders of magnitude for this particular data length and sample rate.

An important factor to consider with this method is that a large amount of computer memory is required to store one or more $N_d \times N_d$ matrices. This is especially important when analyzing long signals such as neutron-star-black-hole (NSBH) and binary neutron star (BNS) mergers. Because of this and the expected increase in run time for longer signals, we only implement this method when analyzing BBH mergers.

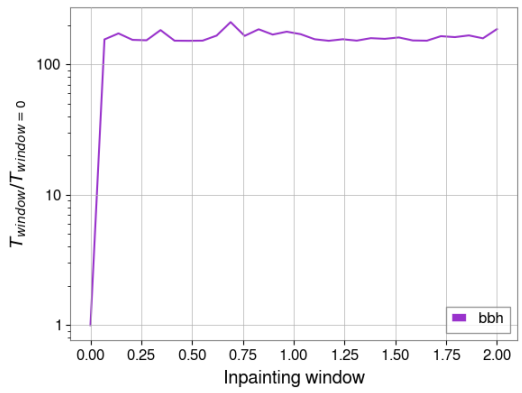


FIG. 3. Increase in evaluation time due to inpainting by directly finding $F$. $T_{window}$ represents the median single-likelihood evaluation time for each window and $T_{window=0}$ represents the median single-likelihood evaluation time without inpainting.

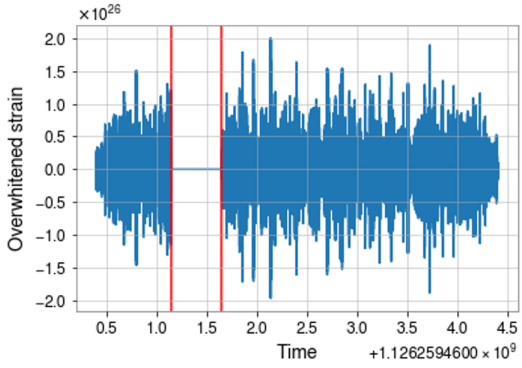


FIG. 4. Overwhitened inpainted data obtained by solving Eq. 8 for $d_{proj}$. Red vertical lines specify the region that was modified.

## B. Solving the Toeplitz system

Fig. 4 shows overwhitened inpainted data that was obtained by solving the Toeplitz system in Eq. 8, for the same segment of data used for Fig. 2. The data inside the hole is effectively zeroed when it is overwhitened.

### 1. *Computational efficiency*

Because $C^{-1}$ is a Toeplitz matrix and because we need only solve Eq. 8 in the hole region, this method can be done in $\mathcal{O}(N_h^2)$ operations using Levinson recursion [8].

Similar to Fig. 3, Fig. 5 shows the increase in evalua-

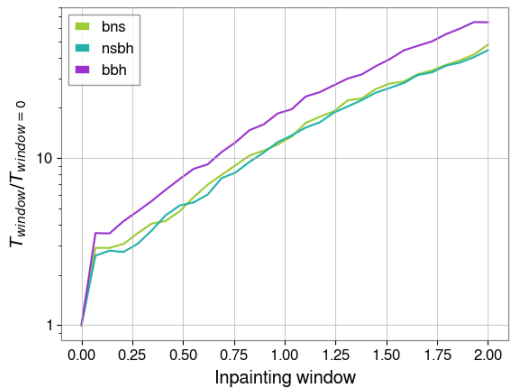


FIG. 5. Increase in evaluation time from inpainting by solving Eq. 8. $T_{window}$ represents the median single-likelihood evaluation time for each window and $T_{window=0}$ represents the median single-likelihood evaluation time without inpainting.

tion times due to inpainting with this method. Because the computational complexity depends on $N_h$ rather than $N_d$, the evaluation time increases for increasing window lengths.

This method requires less memory than storing the $F$ matrix, which allows easier use for analysis of longer signals. Fig. 5 shows how the increase in time compares across BBH, NSBH, and BNS signals. Because BBH signals are typically shorter than BNS and NSBH signals, a larger fraction of them is modified by inpainting, given that the inpainting window is kept constant. BNS and NSBH signals take longer to evaluation, but inpainting is only dependent on data length. This makes the increase in likelihood evaluation time greater for BBH signals, as shown in the plot.

#### 2. *Effect on likelihood evaluations*

`Bilby` calculates the first term in Eq. 10, which is referred to as the *noise log-likelihood*, separately from the last two terms, which are collectively referred to as the *log-likelihood ratio*. Fig. 6 shows how the log-likelihood ratio was affected by increasing the inpainting window.

With windows closer to 0, the variance in the likelihoods is greater. This aligns with what is expected of different waveforms being sampled against the data and some being more well-fitting than others. When the entire segment of data is inpainted, there is no data that contributes to the likelihood and the log-likelihood ratio approaches 0, as shown in the plot.

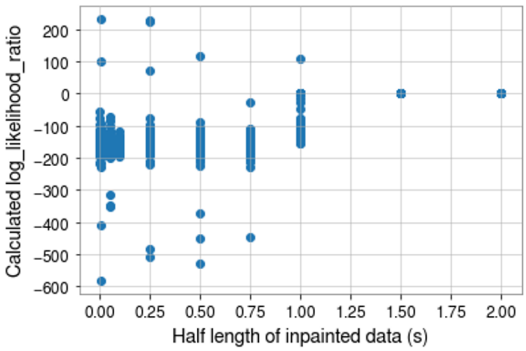


FIG. 6. Calculated log-likelihood ratios for different inpainting windows. Each point represents a single sample in the parameter space.

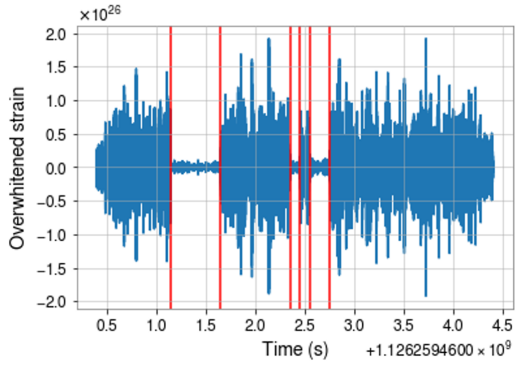


FIG. 7. Overwhitened data obtained by solving Eq. 8 individually for multiple segments. Data produced is incorrectly inpainted. Red vertical lines show the specified limits of each hole.

### C. Inpainting multiple segments

Eq. 8 is, in practice, only solved in a single hole region, which allows the effective use of Levinson recursion to solve the Toeplitz system. However, when multiple segments of data are to be inpainted, each hole contributes to the final solution. Solving Eq. 8 for each hole region individually produces incorrect results. This is shown in Fig. 7, where three segments of data were inpainted at three different regions with different window lengths by solving Eq. 8 for each one. The overwhitened data is not zeroed in the holes because the solution in each segment fails to take into account the existence of other holes.

If one were to solve Eq. 8 at every hole at once, the computational complexity would increase, and the efficiency that was gained from having a Toeplitz system is lost.

To inpaint multiple segments, we use the $F$ matrix, since this method can take every hole into account si-

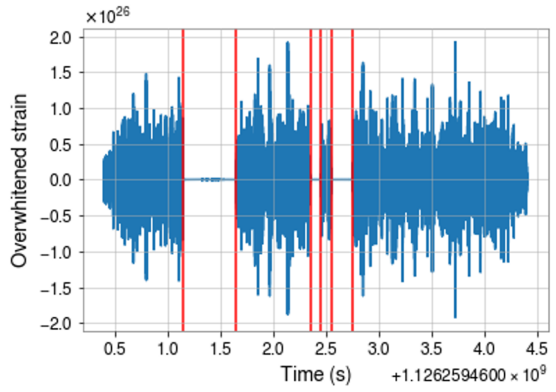


FIG. 8. Overwhitened data with multiple inpainted segments obtained by solving for F matrix. Red vertical lines show the specified limits of each hole.

TABLE I. Fixed parameters for GW150914.

| Parameter | Value |
|---|---|
| a_1 | 0.0 |
| a_2 | 0.0 |
| tilt_1 | 0.0 |
| tilt_2 | 0.0 |
| phi_12 | 0 |
| phi_jl | 0 |
| dec | -1.2232 |
| ra | 2.19432 |
| theta_jn | .89694 |
| psi | 0.532268 |
| luminosity_distance | 412.066 |

multaneously. Fig. 8 shows a segment of data inpainted at three different regions with different window lengths by applying the $F$ matrix. The data produced is approximately zero in the holes when overwhitened, as we require.

### D. PE runs with inpainting

Short PE runs have been completed for GW150914 both by finding $F$ and by solving Eq.8. We only sample merger time, phase, chirp mass and mass ratio for a quick analysis. A full list of the values used for fixed parameters is shown in Table I.

To ensure that our implementation of these methods does not adversely affect the performance of `Bilby`, we inpaint the data 1 second before merger time with a window of 0.25 seconds. Inpainting a short segment with a large time offset from merger time such as this one should not significantly affect the posterior distributions obtained.

Fig. 9 shows the posterior distributions obtained for chirp mass, and Fig. 10 shows those obtained for mass ratio using each inpainting method discussed. Neither of the two inpainting methods negatively affected `Bilby`'s ability to recover significant posteriors.

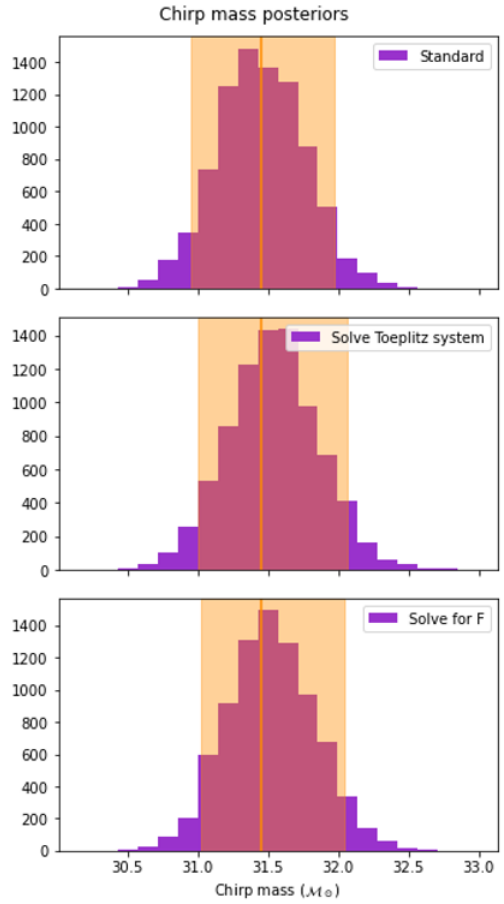


FIG. 9. Posterior distributions obtained for chirp mass, without the inpainting filter applied, with the inpainted data obtained by solving Eq. 8, and with the inpainted data obtained by directly solving for the filter F. Data was inpainted 1 second before merger with a window of 0.25 seconds. Orange vertical line shows accepted value. Orange shading shows 90% credible interval.

Fig. 11 shows the posterior distributions obtained for the geocentric time of the signal. The distribution time for the run with the inpainting filter applied 1 second before the merger time appears to match with that of the standard analysis. However, the distribution for the run with the inpainting filter applied 0.1 seconds before the merger time appears to be slightly shifted right. Geocentric time may be one of the parameters more sensitive to inpainting since bandwidths in the signal that are vital for accurate recovery may be removed with the filter.

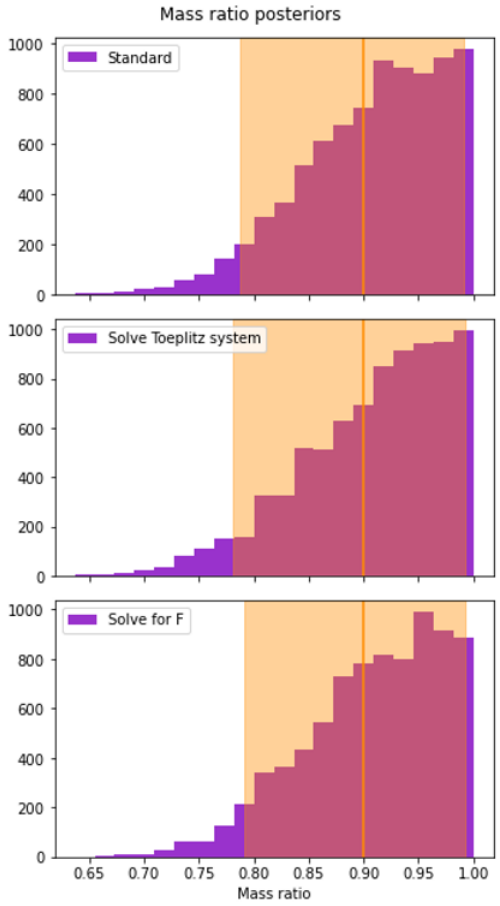


FIG. 10. Posterior distributions obtained for mass ratio, without the inpainting filter applied, with the inpainted data obtained by solving Eq. 8, and with the inpainted data obtained by directly solving for the filter F. Data was inpainted 1 second before merger with a window of 0.25 seconds. Orange vertical line shows accepted value. Orange shading shows 90% credible interval.

## III. PROBLEMS ENCOUNTERED

One of the main problems that we face with this project is the significant run time that inpainting adds to our analyses. Although we would like to test our implementation for numerous test cases, with the current run time of the code we must reconsider how many are feasible for this summer. We considered using different computational resources outside of the CalTech Computer Cluster, but this introduced new problems. Our next attempt to deal with this problem will involve running a standard analysis and then reweighting the obtained samples with an inpainted analysis, based on a process described in [9].

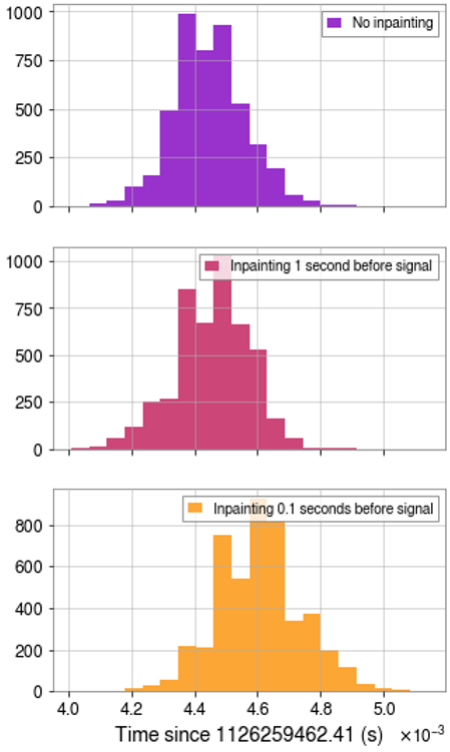


FIG. 11. Posterior distributions obtained for geocentric time without the inpainting filter applied, with the filter centered 1 second before merger with window of 0.1 seconds, and with the filter centered 0.1 seconds before merger with window of 0.05 seconds.

## IV. FUTURE WORK

With our current understanding of how inpainting increases the run time of PE runs, we can prepare a set of injections to determine how often `Bilby` recovers parameters within a specific confidence interval. We will most likely only sample masses, geocentric time, and phase to keep the runs short.

Once we have shown that this implementation works correctly, we will prepare the code to be officially added onto `Bilby`. As a long term goal. the code will also be added to `Bilby_PIPE`, which is an automation of `Bilby` that provides command-line tools for gravitational-wave inference [3].

## V. ACKNOWLEDGEMENTS

I am very thankful for my mentor, Derek Davis, and the work that they have put into making this summer rewarding for both of us. I would also like to thank the LIGO group at the California Institute of Technology

for the positive work environment that they have provided. I gratefully acknowledge the National Science Foundation, the Student-Faculty Programs office, and the LIGO Summer Undergraduate Research Fellowship for making this experience possible.

[1] D. Davis and M. Walker, Detector Characterization and Mitigation of Noise in Ground-Based Gravitational-Wave Interferometers, Galaxies **10**, 12 (2022).

[2] G. Ashton *et al.*, BILBY: A user-friendly Bayesian inference library for gravitational-wave astronomy, Astrophys. J. Suppl. **241**, 27 (2019), arXiv:1811.02042 [astro-ph.IM].

[3] I. M. Romero-Shaw *et al.*, Bayesian inference for compact binary coalescences with bilby: validation and application to the first LIGO–Virgo gravitational-wave transient catalogue, Mon. Not. Roy. Astron. Soc. **499**, 3295 (2020), arXiv:2006.00714 [astro-ph.IM].

[4] B. P. Abbott *et al.* (LIGO Scientific, Virgo), A guide to LIGO–Virgo detector noise and extraction of transient gravitational-wave signals, Class. Quant. Grav. **37**, 055002 (2020), arXiv:1908.11170 [gr-qc].

[5] J. Y. L. Kwok, R. K. L. Lo, A. J. Weinstein, and T. G. F. Li, Investigation of the effects of non-Gaussian noise transients and their mitigation in parameterized gravitational-wave tests of general relativity, Phys. Rev. D **105**, 024066 (2022), arXiv:2109.07642 [gr-qc].

[6] J. Powell, Parameter Estimation and Model Selection of Gravitational Wave Signals Contaminated by Transient Detector Noise Glitches, Class. Quant. Grav. **35**, 155017 (2018), arXiv:1803.11346 [astro-ph.IM].

[7] B. Zackay, T. Venumadhav, J. Roulet, L. Dai, and M. Zaldarriaga, Detecting gravitational waves in data with non-stationary and non-Gaussian noise, Phys. Rev. D **104**, 063034 (2021), arXiv:1908.05644 [astro-ph.IM].

[8] N. Levinson, The wiener (root mean square) error criterion in filter design and prediction, Journal of Mathematics and Physics **25**, 261 (1946), https://onlinelibrary.wiley.com/doi/pdf/10.1002/sapm1946251261.

[9] E. Payne, C. Talbot, and E. Thrane, Higher order gravitational-wave modes with likelihood reweighting, Phys. Rev. D **100**, 123017 (2019), arXiv:1905.05477 [astro-ph.IM].